23rd International Conference on Renewable Energies and Power Quality (ICREPQ'25)
Tenerife (Spain), 25th to 27th June 2025
Renewable Energy and Power Quality Journal (RE&PQJ)
ISSN 2172-038 X, Volume No.23, September 2025

Towards Cost-Effective and Scalable Fuel Cells: Electrochemical Characterization of a Reference Cell for Material Innovation

F.J. Asensio[1], R. Martínez-de-Ternero[1], M. González-Pérez[1], A. Ordoño[1], A. Villamayor[2] and G. Moreno-Fernandez[3]

[1] Department of Electrical Engineering
Engineering School of Gipuzkoa – University of the Basque Country - UPV/EHU
Avda. Otaola, 29, 20600 Eibar (Spain)
Phone number: +34 943 033014, e-mail: **franciscojavier.asensio@ehu.eus**

[2] Department of Hydrogen Technologies
TEKNIKER, Basque Research and Technology Alliance (BRTA)
C. Iñaki Goenaga, 5, 20600, Eibar (Spain)
Phone number: +34 943 206744, e-mail: **antia.villamayor@tekniker.es**

[3] Technology Research Department - Protio Power SL
Parque Empresarial Boroa Box 17, P2-A4 48340 Amorebieta-Etxano (Spain)
Phone number: +34 917 376409, e-mail: **ma.moreno@protiopower.com**

Abstract. Accurate electrochemical modelling of hydrogen fuel cells (FCs) is essential for performance optimization and comparative analysis of different cell configurations. This study presents the electrochemical characterization of a reference FC with graphite bipolar plates, utilizing voltammetry and electrochemical impedance spectroscopy (EIS). The primary objective is to develop a reliable electrical equivalent model of the reference cell, which will serve as a benchmark for future investigations involving alternative FC designs and materials. A detailed methodology for extracting the electrical model from Nyquist plots is provided, ensuring a robust correlation between impedance characteristics and FC operation. The validity of the proposed model is confirmed through polarization curve analysis, establishing its applicability for predictive diagnostics. Additionally, a comprehensive description of the experimental setup configuration and reference components description is included to facilitate reproducibility and further refinement of FC modelling techniques. The findings contribute to the standardization of EIS-based FC analysis, supporting the development of improved electrochemical models for next-generation hydrogen energy systems.

Key words. Hydrogen Fuel cell (FC), Electrochemical Impedance Spectroscopy (EIS), Voltammetry, Equivalent circuit model, Nyquist plot.

1. Introduction

In the transition towards a decarbonized energy system, hydrogen fuel cells emerge as a promising solution due to their high efficiency and zero emissions, with only water vapor as a by-product. However, for these technologies to be viable on a large scale, it is imperative to improve their efficiency and reduce associated costs.

One of the most significant challenges lies in the reliance on scarce and expensive materials. For example, platinum-based catalysts, commonly used in proton exchange membrane fuel cells (PEMFCs), represent a substantial portion of the total cost, and their limited availability could hinder mass adoption [1].

Additionally, graphite bipolar plates, essential for gas distribution and electrical conduction, pose challenges in terms of cost and weight, affecting efficiency and economic feasibility, particularly in the transportation sector. Search for alternative materials that are abundant, cost-effective, and do not compromise performance is, therefore, a priority in current research. Recent studies have explored non-precious metal-based catalysts and alloy compositions, as well as bipolar plates made from conductive polymer composites or coated metals, aiming to reduce costs and enhance sustainability [2].

A key aspect in evaluating the impact of new developments and materials on PEMFCs is the proper characterization of their behavior. In current literature, numerous studies address this characterization using techniques such as voltammetry and electrochemical impedance spectroscopy (EIS) [3]-[5]. However, they mainly focus on the results obtained, without providing, in most cases, a methodology detailed enough to allow a thorough analysis of the various factors influencing the behavior of the fuel cell (FC). Additionally, identifying the components required to build a test bench that allows for proper development of experimental tests is complicated and requires significant effort.

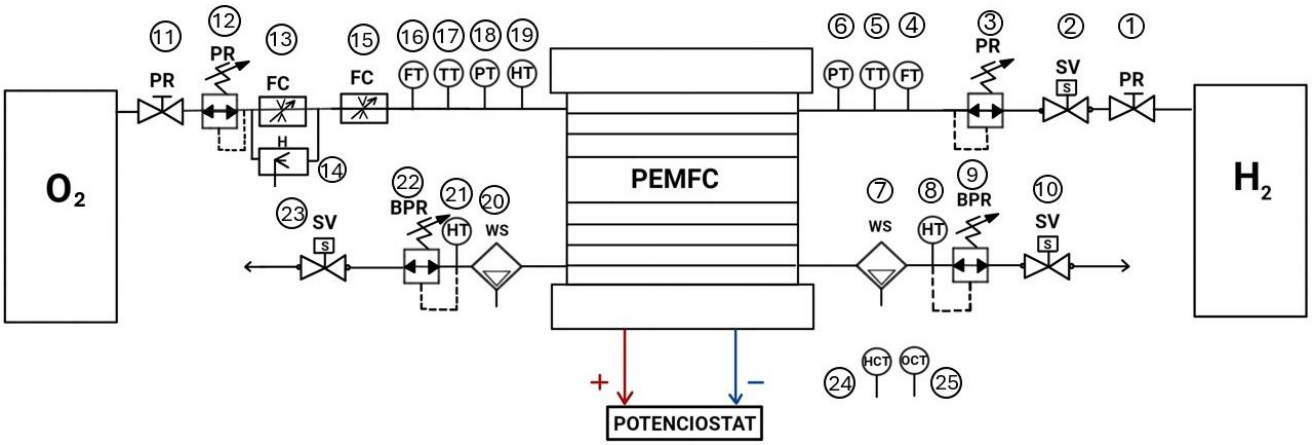

Fig.1. Fuel cell test bench configuration.

In this context, this paper proposes a methodology for the analysis and characterization of FCs using a reference cell equipped with a commercial Membrane Electrode Assembly (MEA) and graphite bipolar plates. In addition, a comprehensive description of the test bench developed to carry out the analyses is provided, so that it can be easily replicated.

The proposed configuration will serve as a standard for objective and quantitative comparisons in future developments incorporating alternative materials. Using voltammetry and EIS techniques, a detailed electrochemical model of the reference cell will be obtained, providing a solid foundation for evaluating the impact of new materials on FC performance and efficiency [6]

2. Test bench and reference cell configuration

This section describes the configuration of the test bench used, as well as the reference FC.

A. Test bench

In FC research, the design and implementation of an effective test bench are crucial for accurately assessing cell performance and behaviour under various conditions. This section provides a comprehensive overview of the test bench utilized in this study, detailing its key components and their respective characteristics. Table I shows the main components that makes up the FC test bench.

Table I. – Test bench components description (Figure 1)

It.	Description	Model	Characteristics
1	PR-Pressure Regulator	PT-LAB10-MV15	Range: 0-16 bar
2	SV-Solenoid valve	Burkert 6013	Supply: 24 VDC Normally closed
3	PR-Pressure Regulator	Bronkhorst P602-CV	Range: 5mbar – 3.2 bar Accuracy: ± 0.5% FS
4	FT-Flow transmitter	Alicat-100SLPM-D	Range: 1-100 slpm Accuracy: ± 0.6% FS
5	TT-Temperature Transmitter	Integrated into (4)	Range: -10 – 60ºC Accuracy: ± 0.75 ºC
6	PT-Pressure Transmitter	Integrated into (4)	Range: 0.8 - 4 bar Accuracy: ± 0.75% FS
7	WS-Water Separator	Hengst Filtration	10 SLPM 0-2 bar
8	HT-Humidity transmitter	Integrated into (9)	Range: 0-100% R.H. Accuracy: ± 0.1%
9	BPR-Backpressure regulator	Alicat PC-100PSIG	Range: 0-2 bar Accuracy: ±0.125% FS
10	SV-Solenoid valve	Burkert 6013	24 VDC Normally closed
11	PR-Pressure regulator	Harris 896	Input: 0-250 bar Output: 0-15 bar
12	PR-Pressure regulator	Bronkhorst P602-CV	Range 5mbar – 3.2 bar Accuracy: ± 0.5% FS
13	FC-Flow Controller	Alicat MC-5SLPM	Range: 0.01-100% FS Accuracy: ± 0.1% FS
14	H-humidifier	O_2 Medical Use	0-20 L/min 0-10 bar
15	FC-Flow controller	Alicat MC-5SLPM	Range: 0.01-100% FS Accuracy: ± 0.1% FS
16	FT-Flow Transmitter	Integrated into (15)	Range: 0-5 slpm Accuracy: ± 0.1% FS
17	TT-Temperature Transmitter	Integrated into (15)	Range: -10 – 60ºC Accuracy: ± 0.75 ºC
18	PT-Pressure Transmitter	Integrated into (15)	Range: 0.8 - 4 bar Accuracy: ± 0.75% FS
19	HT-Humidity transmitter	Integrated into (15)	Range: 0-100% R.H. Accuracy: ± 0.1%
20	WS-Water Separator	Mann+Hummel	20 SLPM 0-2 bar
21	BPR-Backpressure regulator	Alicat PC-100PSIG	Range: 0-2 bar Accuracy: ±0.125% FS
22	HT-Humidity transmitter	Integrated into (21)	Range: 0-100% R.H. Accuracy: ± 0.1%
23	SV-Solenoid valve	Burkert 6013	Supply: 24 VDC Normally closed
24	HCT-Hydrogen concentration transmitter	Xgard M07249	Supply: 8-30 V Range: 0-100% LEL Accuracy: ± 2% FS
25	OCT-Oxygen concentration transmitter	Apogee SO-110	Supply: 12V Range: 0-100% Accuracy: ± 0.01%

The subsequent subsections will elaborate on the following aspects: the configuration of the anode and cathode sides of the test bench, the integration of the

potentiostat, and the instrumentation and data acquisition systems. Each of these elements plays a key role in ensuring precise control and monitoring of the operational parameters of the FC, thereby facilitating reliable and reproducible experimental results.

B.1.Anode Side

The hydrogen supply is based on a system of two V class (99.999%) 50L bottles with a pressure of 200 bar, operating in parallel to increase the autonomy of the tests. The supply pressure is first reduced through a manual regulator (1) to 5 bar and then connected to a solenoid valve (2), whose function is to cut off the hydrogen supply in case of a hydrogen leak or a reduction in the available oxygen concentration in the laboratory. For this purpose, a hydrogen concentration transmitter (24) and an oxygen concentration transmitter (25) are used.

An electronic pressure regulator (3) is connected at the outlet of the solenoid valve (2) allowing a precise control of the hydrogen supply pressure to the FC. A mass flow transmitter (4) is installed between the pressure regulator (3) output and the FC anode inlet. This mass flow transmitter integrates a temperature transmitter (5) and a pressure transmitter (6), which enable monitoring these hydrogen parameters entering the FC. The current test bench configuration only allows testing in dead-end anode mode, since hydrogen recirculation system has not yet been implemented.

At the outlet of the FC anode, the condensed water is removed through a water separator (7) to prevent malfunction of the downstream valves [7]. Next, the backpressure regulator (8) is connected allowing the establishment of a pressure differential between the inlet and outlet. This ensures that when purges are performed through the solenoid valve (9), no deformation occurs in the FC membrane. Additionally, the backpressure regulator (9) also integrates a humidity transmitter (8) to monitor the relative humidity of the purged hydrogen at the FC anode outlet through the purge solenoid valve (10).

B.2. Cathode Side

The cathode supply is based on a V class (99.999%) 50L oxygen cylinder at pressure of 200 bar. To set an appropriate pressure setpoint for the tests, it is first reduced using a manual regulator (11), in the same way as with hydrogen, preventing control issues when using a dual-loop system alongside the mass flow controller [8].

Next, an electronic pressure regulator (12) is connected to stablish a precise pressure setpoint during the tests. To manage the humidity entering the FC, part of the oxygen is circulated through another mass flow controller (13), which is connected in series with the pressure regulator (12) and directly controls the amount of dry oxygen entering the FC. Additionally, in parallel with this mass flow controller (13), a bubbling-type humidifier (14) is installed. This humidifier is heated with an electric resistor, generating vapor to enhance gas humidification.

Following, a second mass flow controller (15) ensures a precise adjustment of the oxygen stoichiometry for the tests, while also providing the flowrate (16), temperature (17), pressure (18) and relative humidity (19) of the reactant through the integrated sensors.

The cathode outlet follows the same configuration as the anode, including condensate separation (20), a backpressure regulator (22) with a humidity transmitter (21). Finally, a solenoid valve (23) is installed to control oxygen purging in case of closed-cathode mode operation.

B.3. Potenciostat

A potentiostat (Kolibrik PTC-0520E) is used at the FC outlet to carry out various tests. This potentiostat allows performing different types of experiments, including:

- Closed Circuit Operation: A constant voltage or current is applied while monitoring the resulting current or voltage, respectively.
- Amperometry/Voltammetry: This test allows for the determination of the polarization curve of the FC, enabling both sweeps, voltage and current.
- Electrochemical Impedance Spectroscopy (EIS): This diagnostic tool analyzes in the frequency domain using the Nyquist diagram the factors that determine the overall efficiency of the FC. In this sense, it can be analyzed the electrode composition and structure, membrane characteristics, and parameters controlled from the test bench, such as humidity or cell pressure.

B.4.Labview Control

Data collection and process control are managed via LabVIEW software and a NI cDAQ-9172 data acquisition device including analog input modules for monitoring sensor data and digital outputs to control the actuators and solenoid valves.

Figure 2 shows the program of the control panel. The control panel includes a cooling circuit that was not required for the tests shown in this paper.

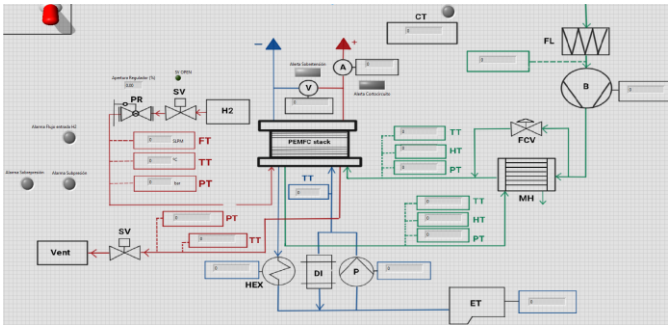

Fig.2. Labview control panel.

B. Reference fuel cell

The reference FC has been constructed using commercially available components [9]. Table II provides

the commercial model and main characteristics of each element that makes up the cell.

Table II. – Reference fuel cell configuration

Element	Description
MEA	Active area: 25 cm^2
Anode Pt charge	0.3 mg/cm^2
Cathode Pt charge	0.5 mg/cm^2
Membrane	Nafion® NRE-212. Thickness 50.8 um. Exchange capacity: ≥0.92 meq/g
GDL	Sigracet 28 BC. Non-woven carbon paper with a Microporous Layer (MPL). PTFE treated to 5 wt%. Thickness: 235 um.
Sealing	HT6135 Silicon gasketing. Tensile strength: 800 psi. Thickness: 0.01 inch. Durometer: 35A (soft) ±5
Plates	Graphite plate with serpentine flow pattern. Dimensions: 9.6x9.6x1.9 cm.

3. Experimental analysis

Since the relative humidity control, as well as the oxygen and hydrogen stoichiometry control are still being fine-tuned, no control over these variables has been implemented. In this context, the FC has operated based on membrane self-humidification, and the reactants have been supplied with both the anode and cathode closed, so that stoichiometric ratios were kept at unity.

Additionally, electric resistances have been attached to the exterior of the plates to control the FC temperature during the tests, which has been maintained at around 60ºC. This significantly improves performance by enhancing moisture distribution and facilitating condensate purging [10].

Figure 3 shows thermal images of the temperature distribution along the FC. It can be observed that, despite the temperature reached by the electric resistances located on the exterior exceeds 100ºC, the average temperature inside the FC remains constant at 60ºC.

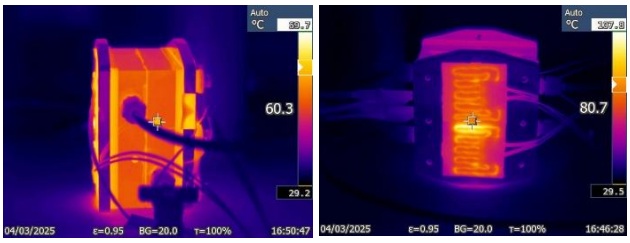

Fig.3. Thermal image of the FC during operation.

Several tests have previously been conducted to determine the optimal torque for the screws that assemble the plates and MEA. To do this, the torque of the screws has been adjusted from 6 Nm to 12 Nm, monitoring the current generated by the FC at a voltage of 0.7 V. These tests were carried out at ambient pressure. Figure 4 shows the relative improvement of the current generated as a function of the torque, with the base current density at 6 Nm being 0.02 A/cm^2.

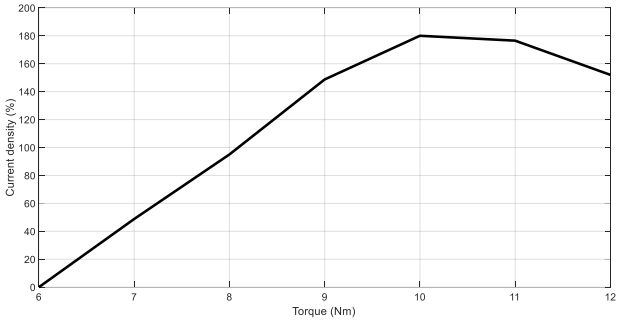

Fig.4. Current density performance as a function of the torque.

The optimal operating point has been obtained at a torque of 10 Nm, resulting in a relative improvement of around 180% compared to the baseline case (6 Nm). The reduction in current density after a certain torque is applied may be due to a decrease in permeability in the electrodes, as well as the loss of electrical contact due to the deformation of the electrode layers and the membrane.

Once the optimal torque was determined, an experimental analysis was developed to determine the influence of the reactant pressure on the behavior of the FC. In this regard, Figure 5 shows the result of the improvement in the current produced by the FC as a function of the variation in the reactant pressure from 1 bar to 1.5 bar absolute. The current data were recorded by setting a terminal voltage of 0.7 V across the FC. The base current recorded for the baseline case (1 bar) was 0.036 A/cm^2.

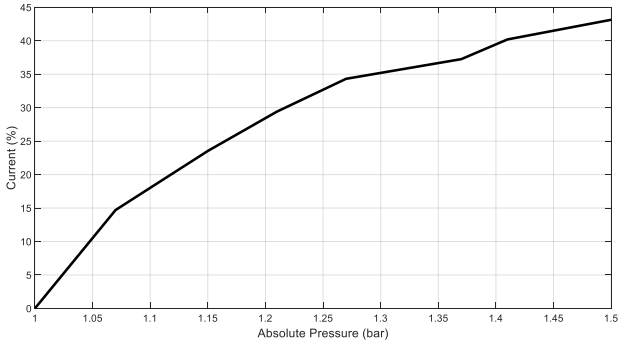

Fig.5. Current density relative improvement as a function of the reactants pressure.

Figure 6 depicts the polarization curve of the FC obtained through an amperometry test with a current sweep from open circuit to 5 A (from 0 to 0.2 A/cm^2).

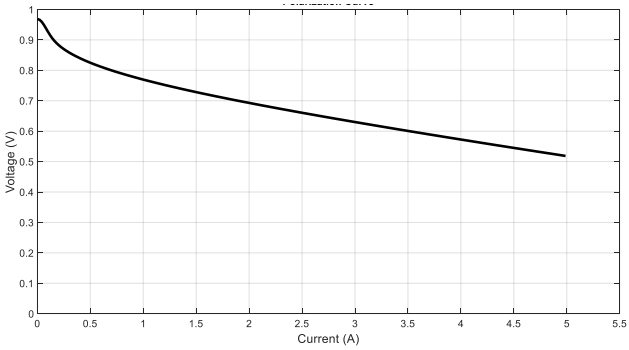

Fig.6. Fuel cell polarization curve.

Figure 7 shows the Nyquist diagram obtained as a result of the EIS analysis. The frequency sweep was performed from 10 kHz to 100 mHz. The voltage amplitude during the test was 10 mV.

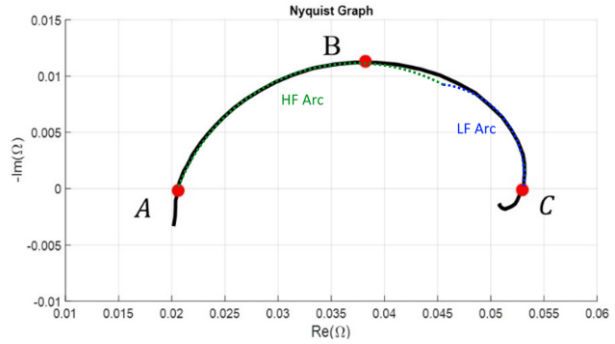

Fig.7. Nyquist plot from the EIS (10 kHz to 100 mHz).

Two arcs can be identified in the Nyquist graph: HF Arc and LF Arc. The first corresponds to the high-frequency (HF) region of the spectrum and is partially associated with charge transfer processes, specifically the movement and accumulation of electric charges at the electrode–electrolyte interfaces. This arc is more prominent at low current densities and tends to decrease as the current increases. Higher compression improves the contact between the GDL and the catalyst layer, which facilitates electron transfer and consequently reduces the HF arc [11]. At lower frequencies (LF), the spectrum displays another characteristic arc, linked to mass transport phenomena, mainly the diffusion of reactants from the flow channels to the catalyst layer. This arc tends to grow with increasing current density due to the reduced efficiency of gas diffusion. When high mechanical compression is applied, the pore size in the GDL beneath the channels can decrease, which further hinders diffusion and leads to an increase in the LF arc [12].

At the high-frequency end of the impedance spectrum (from 10 kHz to 1 kHz), an inductive-type phenomenon can be observed that is not directly related to the FC itself or its electrochemical processes. This behaviour is associated with the wiring and electrical connections of the test bench system and is reflected in the spectrum as a crossover toward the positive imaginary axis (segment below point A). At the lowest end of the spectrum (segment below point C) a pseudo-inductive loop can be identified, the nature of which is still under investigation [13].

4. Fuel cell characterization

Figure 8 shows the Randles electrical circuit used for the characterization of the cell.

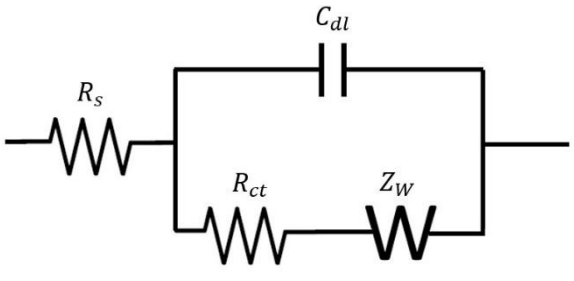

Fig.8. Randles electrical circuit

The Randles electrical circuit is an equivalent model used to interpret the electrochemical response of a FC. It provides key information about the charge transfer resistance R_{ct}, the electrolyte resistance and ohmic resistance R_s, the double-layer capacitance C_{dl} and the Warburg element W, which represents the diffusion of species at the electrode-electrolyte interface. However, to prevent potential damage to the membrane, the Warburg region is not fully developed during the tests shown in this paper.

This model is commonly used in EIS to analyze reaction kinetics and material properties in electrochemical cells, allowing the evaluation of their efficiency and behavior under different operating conditions [14].

The Internal resistance R_s represents the opposition to the flow of protons through the polymer membrane, as well as the electrons through the plates and electrodes. This parameter is crucial because it is directly related to the ionic conductivity of the membrane and, therefore, to the performance of the cell. Since membrane conductivity is directly proportional to humidity, a lower R_s corresponds to higher conductivity.

In the previous test (figure 7), the electrolyte resistance (corresponding to the first intersection of the semicircle with the real axis, designated as point A) is 0.0206 Ω.
The charge transfer resistance R_{ct} quantifies the resistance during the electron transfer process between the electrolyte and the electrodes. An increase in R_{ct} results in a slower reaction rate, offering insights into the reaction kinetics and the performance of the cathode-side catalyst. Moreover, an escalating R_{ct} is associated with a reduction in the potential (φ), which leads to a decrease in temperature and, consequently, diminishes the air or oxygen stoichiometry.

This resistance is determined by the difference between the second and the first intersection points of the semicircle with the real axis (figure 7), as shown in the following expression:

$$R_{ct} = R_c - R_s \tag{1}$$

where R_c correspond to the second intersection of the semicircle with the real axis of the Nyquist graph (point C in figure 7). In the test carried out has a value of 0.053 Ω, so that R_{ct} is 0.0324 Ω.

The double-layer capacitance C_{dl} represents the equivalent capacitance of the double-layer, corresponding to the charge accumulated at the electrode–electrolyte interface. It is calculated using the expression:

$$\boldsymbol{C_{dl} = \frac{1}{R_{ct} \cdot \omega_c}} \tag{2}$$

To determine ω_c, the frequency at the highest point of the semicircle (indicated as point C in figure 7) is used. The highest point corresponds to an imaginary value of the impedance of 0.011215 Ω, which is given at a frequency of 31.623 Hz. Therefore, ω_c is calculated as follows:

$$\omega_c = 2 \cdot \pi \cdot F \tag{3}$$

Evaluating (3) it is obtained a ω_c of 198.69 rad/s, and substituting into equation (2) yields a C_{dl} of 155.335 mF.

These parameters serve as a baseline, considering the elements used to build this reference cell (Table II). In this sense, if any parameter or component in the reference cell is modified (such as platinum loading, membrane or GDL composition, materials and coatings of the plates, etc.), it is possible to determine the effect on the performance of the cell by observing how each parameter of the Randles circuit is affected.

5. Conclusion

This paper has presented a complete methodology for the electrochemical characterization of a hydrogen fuel cell using EIS and voltammetry. A set of commercially available reference components has been defined to ensure the reproducibility of the tests and the electrochemical model obtained, facilitating objective and quantitative comparisons in future studies.

Once the humidity and stoichiometry control loops are implemented, more detailed analyses will be possible. In this regard, one of the objectives for future developments is to analyze the variation of the ionic resistance as a function of the tightening torque through EIS tests. Additionally, it will be possible to obtain optimal stoichiometry maps for each operating point of the cell.

The next step in this research will focus on evaluating the performance of metallic bipolar plates made of 316L stainless steel with various Nb-carbon-based coatings. Additionally, the impact of different reactant gas flow channel designs on fuel cell efficiency will be analyzed. The effectiveness of these developments will be compared with the results obtained for the reference cell established in this study, contributing to the advancement of more efficient, durable, and cost-effective fuel cell systems for large-scale implementation in the energy transition.

Acknowledgement

Authors thank for the support received from the Ministry of Industry and Tourism of Spain (grant for projects of hybrid vehicles and electric vehicles with batteries and hydrogen fuel cells, HIB-01-07-2023).

References

[1] T. S. Andrade and T. Thiringer, "Low platinum fuel cell as enabler for the hydrogen fuel cell vehicle," *J. Power Sources*, vol. 598, pp. 234140, 2024.

[2] C. Windarto, U. K. Chanda and O. Lim, "A review of materials and surface processing for bipolar plates in polymer electrolyte membrane fuel cells," *Int J Hydrogen Energy*, vol. 92, pp. 419–433, 2024.

[3] X. Tao, Z. Zeng, H. Liu, M. Suo, Q. Li, K. Sun, Z. Che and T. Wang, "PEM fuel cell with non-uniform porous metal foam as cathode flow field," Applied Energy, vol. 380, pp. 124938, 2025.

[4] D. Mitra, K. Heinrich, S. Gierse, C. Zeiner, F. Siegel, A. Willert and R. Zichner, "Direct deposition of catalyst layers on polymer electrolyte membrane (PEM) for fuel cells with controlled platinum distribution by inkjet printing," Int. J. Power Sources, vol. 638, pp. 236503, 2025.

[5] Ghorbani, J. De Vaal, G. Afonso and K. Vijayaraghavan, "Use of reduced-voltage EIS to establish a relation between oxygen concentration and EIS responses of large commercial PEM fuel cell modules," Int J Hydrogen Energy, vol. 48 (84), pp. 32654-32671, 2023.

[6] X. Wu, S. Xing, J. Luo, H. Wang, F. Huang and C. Zhao, "Progress and Challenges on Air-cooled Open-cathode Proton Exchange Membrane Fuel Cells: Materials, Structures, and Systems," *Energy Reviews*, pp. 100130, 2025.

[7] U.S. Department of Energy. (2004). Fuel Cell Handbook. Office of Energy Efficiency and Renewable Energy, Available: https://www.netl.doe.gov/sites/default/files/netl-file/FCHandbook7.pdf

[8] R. O'Hayre, S.W. Cha, W. Colella and F.B. Prinz, "Concurrent use of an electric pressure regulator and a mass flow controller can cause control conflicts and tuning challenges", Fuel cell fundamentals, ISBN: 9781119113805, 2016.

[9] *Fuel Cell Store*. Available: https://www.fuelcellstore.com/fuel-cell-components.

[10] Weber, A. Z. and Newman, J., "*Modeling Transport in Polymer-Electrolyte Fuel Cells*," Chemical Reviews, vol. 104, pp. 4679–4726, 2004.

[11] G. Dotelli, L. Omati, P. Gallo Stampino, P. Grassini, and D. Brivio, "Investigation of gas diffusion layer compression by electrochemical impedance spectroscopy on running polymer electrolyte membrane fuel cells," J Power Sources, vol. 196, pp. 8955-8966, 2011.

[12] C. Zhao, S. Xing, W. Liu, M. Chen, Y. Wang and H. Wang, "An experimental study on pressure distribution and performance of end-plate with different optimization parameters for air-cooled open-cathode LT-PEMFC," Int J Hydrogen Energy, vol. 45 (35), pp. 17902-17915, 2020.

[13] I. Pivac and F. Barbir, "Inductive phenomena at low frequencies in impedance spectra of proton exchange membrane fuel cells - a review," J Power Sources, vol. 326, pp. 112-119, 2016.

[14] M. A. Rubio, A. Urquia, R. Kuhn and S. Dormido, "Electrochemical parameter estimation in operating proton exchange membrane fuel cells," *J. Power Sources*, vol. 183, *(1)*, pp. 118–125, 2008.